Condition Monitoring of Wind Turbine Blades Using MEMS Accelerometers

Ozak O. Esu*, James A. Flint and Simon J. Watson

*Correspondence; O.O.Esu@lboro.ac.uk

School of Electronic, Electrical and Systems Engineering

Loughborough University

Loughborough

Leicestershire

LE11 3TU

United Kingdom

Abstract

Wind turbine rotors in operation are subject to fatigue which is reflected as cracks and delamination in composite blades. Blade condition monitoring is becoming important to operators and insurers alike as the cost of damaged-blade repairs or replacement is very high and hence, the need for cheaper long-term solutions in the current strives for sustainable energy. In this paper, vibration/modal analysis non-destructive testing (NDT) method was used in conjunction with Signal Processing techniques to investigate the feasibility of integrating low-cost micro electro-mechanical systems (MEMS) accelerometers for blade condition monitoring as an alternative to the conventional piezoelectric accelerometers which are bulky and expensive. A rig-mounted 4.5m long blade from a 25kW Carter wind turbine was retrofitted with five MEMS accelerometers of type ADXL335 and vibration response measurements were recorded and analysed as the blade's angle of orientation was changed by 10° from 0° to 180°. Results showed that the MEMS accelerometers are capable of measuring the blade response at each set angle of orientation. This shows potential for MEMS accelerometer integration for condition monitoring as in reality, wind turbine blades will continuously be in rotation in order to generate energy. Thus these accelerometers can perform as normal when there is a change in the blade's orientation. In conclusion, MEMS accelerometers have a great potential to be integrated easily either retrofitted externally or embedded in blades at manufacture for condition monitoring at marginal cost.

1 Introduction

Condition monitoring (CM) which triggers subsequent maintenance actions is an important strategy for minimising breakdown whilst avoiding periodic assessment and associated downtime. It is a preventive type of maintenance based on the actual health of the system [1]. At a general level, condition monitoring can be described as a management tool which provides information about the likely future performance-or lack of it-of a component of a wind turbine such as the blade, or even the entire wind turbine system [2]. The reason for introducing condition monitoring of the blades is that there is a high-level of uncertainty in predicting the health of a wind turbine blade during its lifetime. This uncertainty stems from manufacturing tolerances and the different stresses and strains experienced by the blade in its lifetime. It is difficult to predict damage development within the blade structure and in which of the rotor blades on a given turbine the damage will occur. It is therefore desirable to monitor all of the blades separately and respond by performing detailed inspections of the blades when condition monitoring systems implemented indicate [3], [4] .

Experiments conducted in this paper are a continuation of work recently carried out by Esu et al. [5] which showed that MEMS accelerometers have the potential to detect defects and variations in the health of small wind turbine blades when measurements were conducted in the flapwise orientation (0°). As demonstrated in [5], modal analysis (impact testing) [4], [6–10] was used. This is mainly because resonant properties like mass, stiffness and damping properties of mechanical structures such as turbine blades, are directly influenced by its physical properties and hence any changes in its modal parameters such as its natural frequency is potentially useful information for condition monitoring [6], [8].

Measuring vibration is a well-established method for detecting and diagnosing any deviation from normal conditions in rotating mechanical structures which has now being extended to wind turbine blades. However, the use of conventional piezoelectric accelerometers to measure these vibrations is the predominantly used and accepted technology. This paper explores the use of MEMS accelerometers as an alternative to these piezoelectric accelerometers as there are high costs generally associated with the piezoelectric accelerometers especially if simultaneous multiple data collection points are required. These costs are mainly because of the cost of piezoelectric accelerometers and the price of the associated electronic signal conditioning circuits necessary for its use [11], [12].

In order to reduce the cost of vibration-based condition monitoring and with the recent advances in embedded systems technologies, Micro Electro-Mechanical Systems (MEMS) accelerometers have been introduced. They have a built-in signal conditioning unit (in the form of an amplifier and filter) unlike the conventional piezoelectric accelerometers currently in use. They are of low-cost and are of a very small size. Miniaturisation of these MEMS accelerometers has reduced its cost by decreasing material consumption during its manufacture. It has also increased the applicability of MEMS accelerometers as it is possible to place these MEMS accelerometers in places where conventional piezoelectric sensors for this purpose do not fit physically. These characteristics make MEMS accelerometers suitable for vibration monitoring and therefore offer a cheaper alternative to the conventional piezoelectric accelerometers used [11–15].

2 MEMS accelerometers

Although MEMS accelerometers are currently receiving attention for vibration monitoring purposes, they have been in existence for quite some time and are extensively used in other applications such as navigation systems in the automotive industry and in the telecommunications industry for mobile telephones [13], [14]. In fact, the current availability of MEMS accelerometers is as a result of their widespread use in these applications and this has dramatically pushed down their cost [5].

MEMS accelerometers are usually classified as piezoresistive and capacitive based accelerometers.

2.1 The piezoresistive MEMS

Conventional piezoelectric accelerometers generally consist of a single-degree of freedom system of mass suspended by a spring. In piezoresistive MEMS accelerometers, there is typically a cantilever beam with a proof mass located at the tip of the beam and a piezoresistive patch on the beam web. The schematic of a piezoresistive MEMS accelerometer is shown in Figure 1. The movement of the proof mass when subjected to vibration, changes the resistance of the embedded piezoresistor. The electric signal generated from the piezoresistive patch due to change in resistance is proportional to the acceleration of the vibrating object [11], [12], [16], [17].
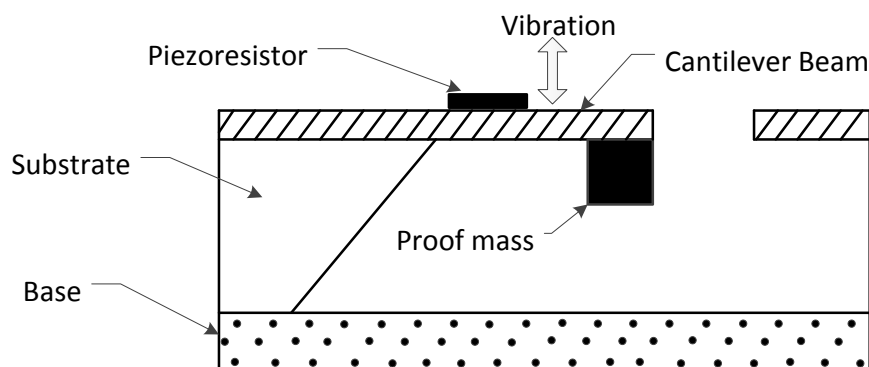

Figure 1 A typical MEMS piezoresistive accelerometer using cantilever design adapted from [11] .

2.2 The capacitive based MEMS

The capacitive based MEMS accelerometers measure acceleration based on a change in capacitance due to a moving plate or sensing element. This is the most commonly implemented MEMS accelerometer because they generally offer more sensitivity (more mV/g) and more resolution than equivalent piezoresistive accelerometers [18]. A capacitive-based MEMS is therefore chosen for the experiments in the current paper. The schematic of a capacitive MEMS accelerometer is shown in Figure 2 below [11], [12], [14], [16], [19].
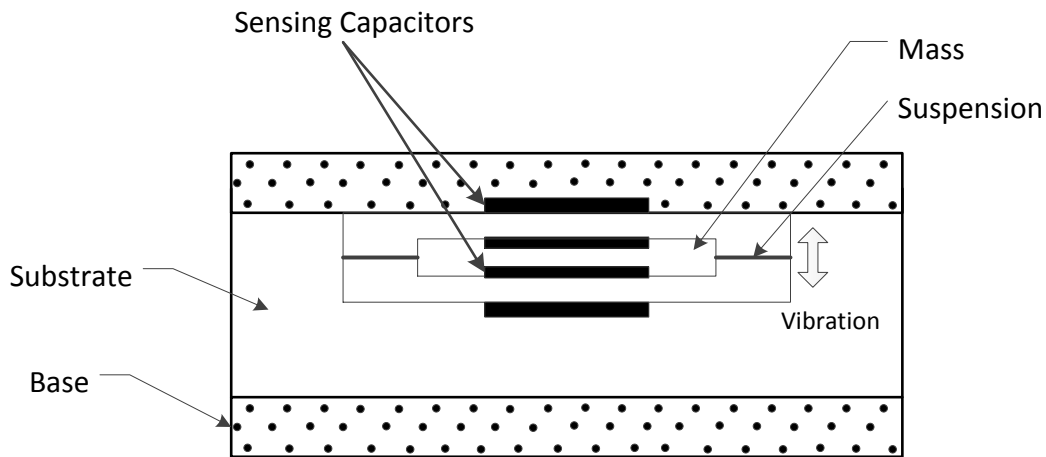
Figure 2 A typical capacitive based MEMS accelerometer based on membrane design adapted from [12].

3 Testing and results

Five printed circuit board mounted ADXL335 [20] accelerometers were glued to a 4.5m long tapered blade taken from a 25kW Carter wind turbine [21] along its flat horizontal surface ensuring that at least one accelerometer was placed at one of the three defined degrees of freedom of turbine blades. A specialist support was constructed from steel box-section beams which allowed the blade to be supported above the ground using its usual mechanical fixings. The support also allowed the blade to be rotated about its axis.

3.1 Accelerometer fixing positions

Degrees of freedom (DOF) describe the number of possible motion and direction; and each DOF is characterized by a direction and position. The mode shapes of a blade are generally assumed to be described by deflection in the *flapwise* and *edgewise* directions. *Torsion* is assumed to be described by rotation of the chord about the pitch axis. The rigid body motion can therefore be described by three degrees of freedom (DOFs) on the turbine blade; two flapwise DOFs describe the flapwise and torsion, and one edgewise DOF describes the edgewise deflection [9], [10]. Figure 3 below illustrates the three DOFs along the cross-section of a turbine blade where accelerometers were placed during testing.
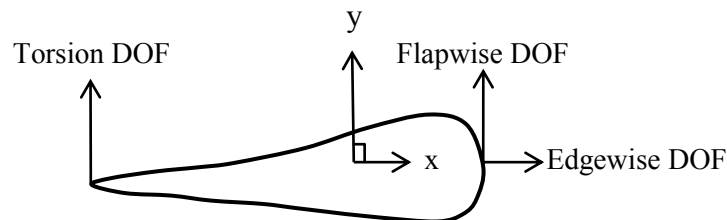

Figure 3 Cross section of blade showing the three degrees of freedom.

Connection wires were taped to the blade surface to minimise unwanted vibrations. An impact hammer (Type 8202) [22] manufactured by Brüel & Kjær which has a built-in force transducer (Type 8200) was connected to a charge amplifier [23] and was used to strike the 4.5m long blade at a fixed-point close to the blade's tip at all angles of orientation set. The

purpose of the charge amplifier was to convert the signal from the force transducer into a useful voltage signal measurable by the 16-channel NI USB-6251 Data Acquisition system [24]. This allowed for synchronised measurement of the input from the hammer and output from the accelerometers to be conducted. Transducer sensitivity matching was achieved by calibrating the amplifier using the sensitivity value provided in the calibration chart [22] for the impact hammer force transducer. The DAQ system was set to read five seconds of data at a rate of 20 ksamples/s using NI LabVIEW SignalExpress [25] software. Figure 4 below shows the architecture of the measurement, experiment set-up and accelerometer positions along the 4.5m long turbine blade.

Input to the blade and the vibration response were measured and recorded on the DAQ system. The hammer head weighed 0.28kg, the plastic tip used weighed 0.0039kg and the additional mass attached to the back of the hammer head weighed 0.122kg. This allowed for the pulse duration on blade impact to be regulated. All measurements were post-processed in MATLAB [26].
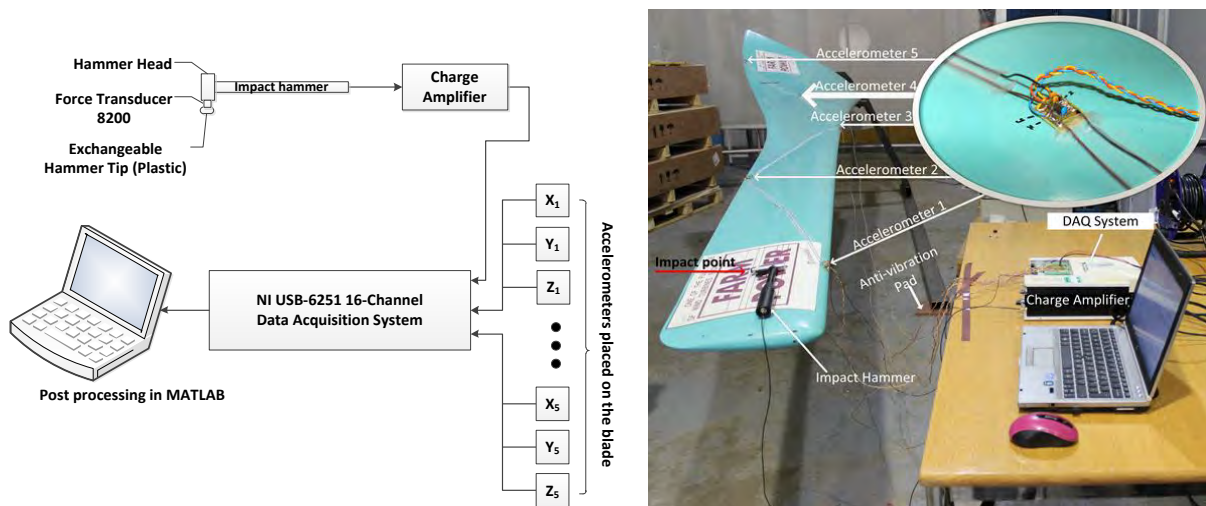

Figure 4 Architecture of experiment, annotated picture showing the experiment set-up; zoomed-in section of one of the ADXL335 accelerometers, point of impact and accelerometers, point of impact and accelerometer positions along the 4.5m long blade.

3.2 The ADXL335 accelerometer

The ADXL335 [20] accelerometer used in experiments in this paper, is a surface micro-machined device with signal conditioned voltage outputs. It is a small, thin, low power device that can measure the static acceleration of gravity in tilt-sensing applications, as well as dynamic acceleration resulting from motion, shock, or vibration. The accelerometers were mounted on printed circuit boards (PCB) to allow wires to be connected easily, as the accelerometer package itself measured only 4mm × 4mm × 1.45mm. Figure 5 below shows the accelerometer size in comparison to a coin and its axes of sensitivity. It is worth mentioning that the small size of the ADXL335 accelerometer is ideal for vibration monitoring as it allows for possible integration during manufacture without greatly affecting the blade design and vibration characteristics. The ADXL335 measures acceleration in 3-axes with a full-scale range of ±3g, (where g=9.81ms^{-2}) has a typical sensitivity of 300 mV/g, user selective bandwidth with a range of 0.5Hz to 550Hz on the Z_{out} and up to 1600Hz on the X_{out}

and Y_{out}, to suit the application using external capacitors across each of the output pins X_{out}, Y_{out} and Z_{out}, has a 150×10^{-6} g/√Hz rms noise floor across X_{out} and Y_{out} and 300 µg/√Hz rms at Zout and resonant frequency of 5.5 kHz. The power supply is 3.6V maximum and 1.8V minimum [20].
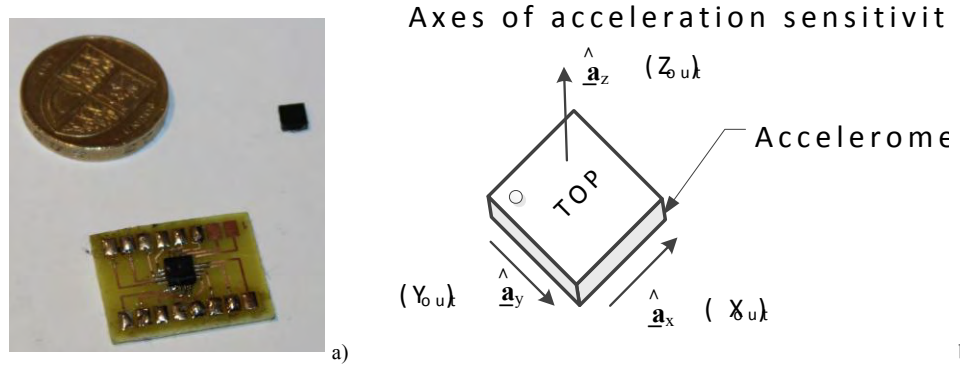

Figure 5 The ADXL335 MEMS accelerometer: a) stand alone and PCB mounted in relation to a UK £1 coin and b) axes of acceleration sensitivity.

3.3 Noise sensitivity

In the research described in this paper, to lower the noise floor and improve the resolution of the ADXL335 accelerometer, low-pass filtering to a bandwidth of 500Hz was implemented by soldering a 0.01 µF capacitor at each of the output pins. A 0.1 µF capacitor was also soldered at the accelerometer supply pins to decouple the accelerometer from noise on the power supply rails. 500Hz was selected as the largest common bandwidth for the 3 axes outputs, not all of which are identical.

The noise floor of the ADXL335 has the characteristics of white Gaussian noise, which contributes equally at all frequencies and is proportional to the square root of the accelerometer bandwidth [20]. As the measurement bandwidth increases, the noise floor increases and the signal to noise ratio (SNR) of the measurement decreases [27]. The typical noise resolution for the ADXL335 with a single-pole was calculated from the following formula given in the datasheet [20];

$$rms\ Noise\ (X_{out}\ and\ Y_{out}) = 150 \times 10^{-6}\ g/\sqrt{Hz} \times \left(\sqrt{BW \times 1.6}\right) \qquad (1)$$

$$rms\ Noise\ (Z_{out}) = 300 \times 10^{-6} g/\sqrt{Hz} \times \left(\sqrt{BW \times 1.6}\right) \qquad (2)$$

where BW is the user set bandwidth. Hence, the minimum noise floor was calculated to be 4.24×10^{-3} g at X_{out} and Y_{out} and 8.49×10^{-3} g at Z_{out}.

The experimental RMS noise floor was measured in the laboratory at each angle of the blade orientation from 0° to 180°. This was done by taking measurements of the initial DC level of each accelerometer when the blade was stationary at each angle of orientation. These measurements were averaged which gave the DC offset values at each output axis of each accelerometer. This DC offset was then subtracted from each axis output taken when the

blade was vibrating in order to set the zero acceleration point and the RMS noise values were calculated in MATLAB [26].

Figure 6 shows a plot of the RMS noise values at each accelerometer output axis against the angle of blade orientation measurements were taken. It is worth noting that each accelerometer position along the blade is not at the reference zero g acceleration position as the blade profile structure varies along the turbine blade. Therefore, the blade angle orientation is not the same as the accelerometer angle of orientation.

The trend observed in Figure 6 was that for all the graphs, the RMS noise tends to be stable between 10° and 160°. However, as the accelerometer position on the blade relative to the point of impact increases, the stability/uniformity of the RMS noise values between 10° and 160° decreases. In simpler terms, accelerometer 1 which is closest to the point of impact appeared more consistent than accelerometer 5 which was the farthest from the impact point between 10° and 160°.

Below 10° and above 160°, variations in RMS noise values were observed at each output axis. However, this was more pronounced at the output axis, Z_{out}. This may be due to the fact that the measurements along this axis correspond to the symmetric axis of the blade along which the excitation/impact was injected. The peak in RMS noise value at 10° in accelerometer 2 may be a numerical or measurement error. However, overall it can be concluded that for the devices measured, the noise was of the same magnitude as that quoted in the manufacturer's data sheet. It should be noted that quoted RMS noise is for a typical device and is not guaranteed.
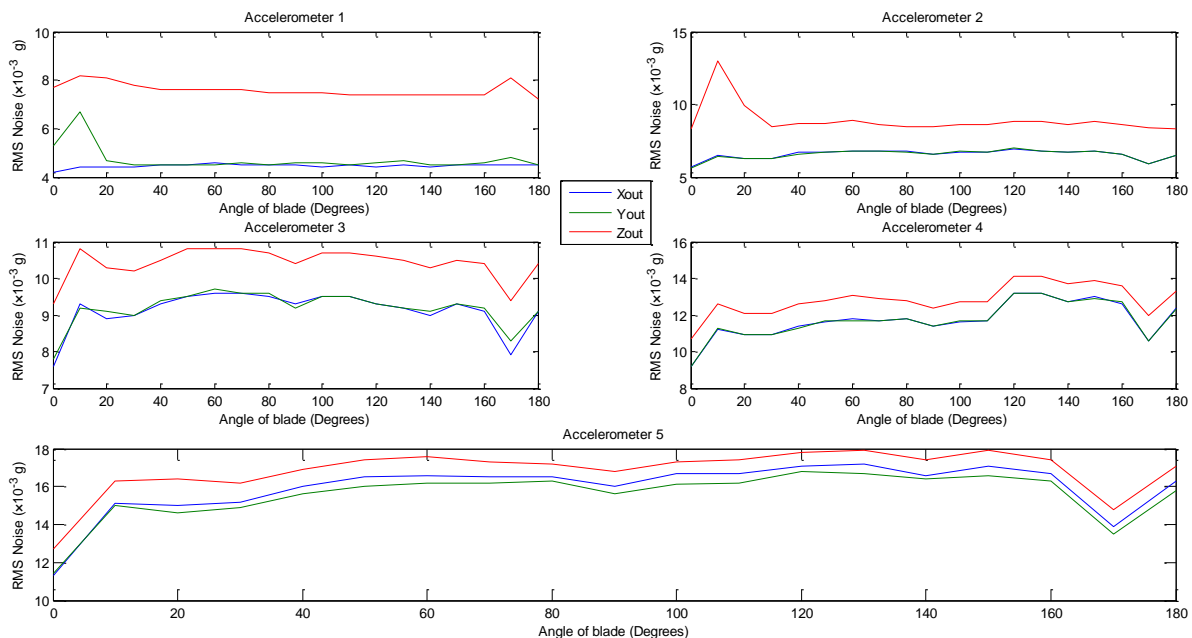

Figure 6 Graph showing the relationship between the measured RMS noise value and angle of blade orientation.

3.4   Further analysis

Figure 7 shows the measured acceleration response from each accelerometer when the blade was struck at a fixed point close to the tip. It also shows the magnitude of the force that was

applied impulsively to the blade. The responses are typically decay type responses as expected for the impulse impact excitation.

At every angle of blade orientation, accelerometers 2 and 4 had the highest signal response while accelerometers 1 and 3 had the lowest signal response. This is in agreement with the logically expected output response, as accelerometers 1 and 3 were positioned along the main spar and leading edge of the blade which has a thicker structure and profile than the trailing edge where accelerometers 2, 4 and 5 were positioned.

Another observed feature of the time domain plots is that Z_{out} had the highest response as it is in parallel with the excitation plane of the blade (see Figure 5).
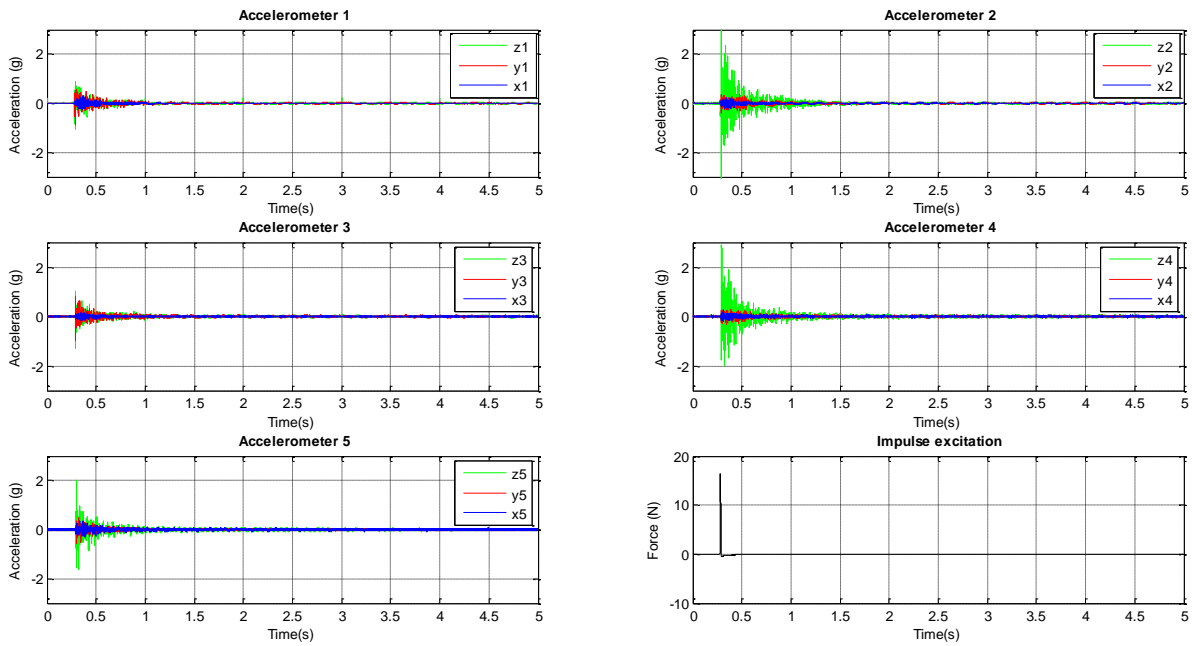

Figure 7 Measured acceleration responses of the MEMS accelerometers and impulse input response.

The resultant acceleration R, was calculated for each of the accelerometers using the equation;

$$R = \sqrt{x_n{}^2 + y_n{}^2 + z_n{}^2} \qquad (3)$$

where x, y and z represent the response measured at each corresponding accelerometer output axis and n is the accelerometer position number. The resultant acceleration signal was windowed and plotted to show the noise floor. Windowing reduces error due to limited duration of the signal when computing the frequency content. Fast Fourier transformation was conducted on the windowed resultant acceleration signals and Figure 8 shows the plots created in MATLAB [26]. The magnitude of all the graphs is relative to a reference of 1g and were normalised with respect to the maximum deflection at accelerometer 2, which had the highest amplitude as shown in Figure 7 above.

The resultant acceleration signals show the frequency modes that were excited clearly above the noise floor as the blade responds to the impulsive excitation from the force hammer. The flapwise natural frequency of the blade was estimated to be 1.6 Hz using the 'snap-back'

principle [9]. The snap-back method is where the turbine blade is deflected at its free-end, from its rest position and a stop-watch is used to count the blade's oscillations. Based on this estimation, the next five frequency modes of the blade were calculated and compared with measured values from Figure 7. Table 1 summarises results obtained.

Mode	Estimated frequency (Hz)	Measured frequency (Hz)
1st	1.6	1.53
2nd	3.2	3.05
3rd	4.8	4.73
4th	6.4	5.95
5th	8.0	7.78

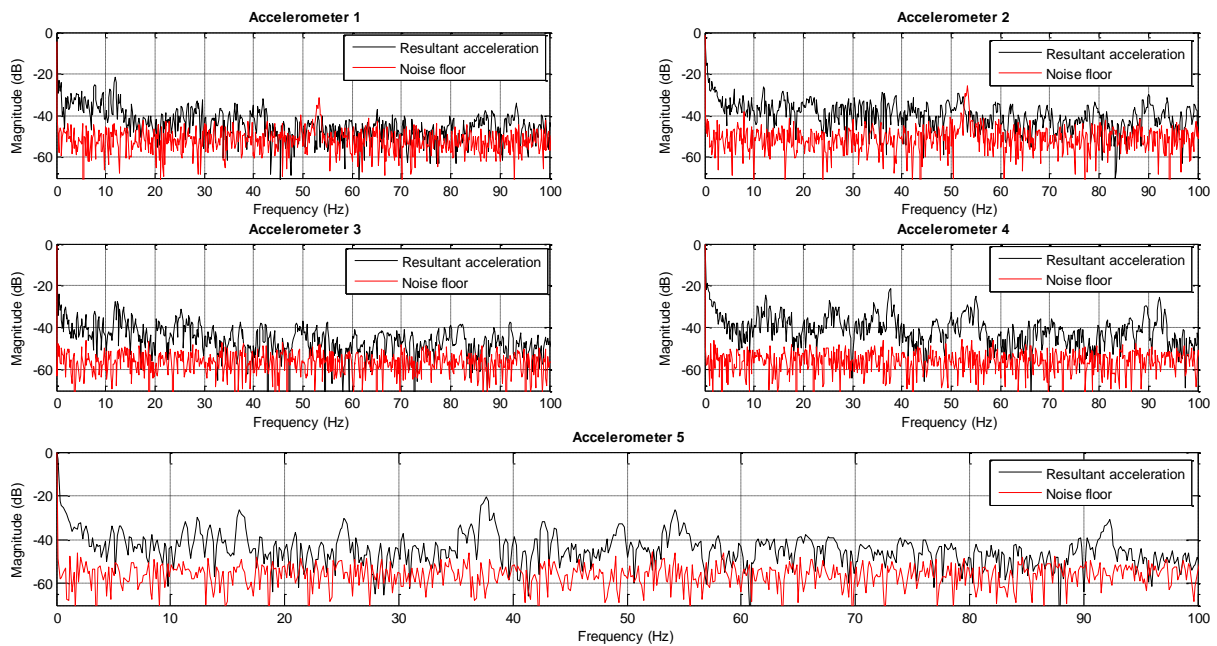**Table 1** Estimated and measured modal frequencies.

Figure 7 Frequency spectrum showing the resultant acceleration and noise measurements for each accelerometer position on the 4.5m long blade for one second data read at a rate of 20 ksamples per second and plots normalised with respect to maximum deflection at accelerometer 2.

4   CONCLUSION

MEMS accelerometers could potentially be good alternatives to standard piezoelectric accelerometers mainly for low cost condition monitoring as they require little external instrumentation and the purchase cost is low. However, the choice of the type of MEMS accelerometer to be used should take into consideration factors such as; sensitivity, amplitude limit, resolution, frequency range and possible environmental factors.

The data collected in experiments showed a significant level of noise contribution with visible peaks in certain bands which are likely to be characteristics of the type of MEMS accelerometer used. Regardless of the noise, which can be easily characterised, modal frequencies were clearly visible above the noise floor within the set bandwidth of measurements. More investigations with various MEMS accelerometers will need to be conducted, with the final goal of a fully embedded instrument for a turbine blade.

5   REFERENCES

[1]   E. Wiggelinkhuizen, T. Verbruggen, H. Braam, L. Rademakers, J. Xiang, and S. Watson, "Assessment of Condition Monitoring Techniques for Offshore Wind Farms," *Journal of Solar Energy Engineering*, vol. 130, no. 3, p. 031004, 2008.

[2]   J. R. McEwan, "Condition Monitoring," in *Condition Monitoring:Proceedings of the 3rd International Conference (Windsor, UK, 15-17 October 1990)*, Illustrate., J. R. & A. McEwan, Ed. Essex, England: Elsevier Applied Science, 1991, pp. 3–35.

[3]   K. K. Borum, M. McGugan, and P. Brøndsted, "Condition monitoring of wind turbine blades," in *27th Risø International Symposium on Materials Science: Polymer Composite Materials for Wind Power Turbines*, 2006, pp. 139–145.

[4]   J. G. McGowan, R. W. Hyers, K. L. Sullivan, J. F. Manwell, S. V. Nair, B. McNiff, and B. C. Syrett, "A review of materials degradation in utility scale wind turbines," *Energy Materials: Materials Science and Engineering for Energy Systems*, vol. 2, no. 1, pp. 41–64, Mar. 2007.

[5]   O. O. Esu, J. A. Flint, and S. J. Watson, "Integration of Low-cost Accelerometers for Condition Monitoring of Wind Turbine Blades," in *European Wind Energy Conference, Vienna*, 2013, pp. 1–4.

[6]   S. Ganeriwala and J. Yang, "Using Modal Analysis for Detecting Cracks in Wind Turbine Blades," *Sound & Vibration*, vol. 45, no. 5, pp. 10–13, 2011.

[7]   S. N. Ganeriwala, V. Kanakasabai, and M. Richardson, "Modes Indicate Cracks in Wind Turbine Blades," *Rotating Machinery, Structural Health Monitoring, Shock and Vibration, Volume 5*, pp. 509–513, 2011.

[8]   B. Schwarz and M. Richardson, "Experimental modal analysis," in *CSI Reliability Week*, 1999, vol. 35, no. 1, pp. 1–12.

[9]   G. C. Larsen, M. H. Hansen, A. Baumgart, and I. Carlen, "Modal Analysis of Wind Turbine Blades (Risø -R-1181(EN))," Denmark, 2002.

[10]   H. B. Pedersen and O. D. Kristensen, "Applied modal analysis of wind turbine blades (Risø -R-1388(EN))," Denmark, 2003.

[11]   A. Albarbar, A. Badri, J. K. Sinha, and A. Starr, "Performance evaluation of MEMS accelerometers," *Measurement*, no. 42, pp. 790–795, 2009.

[12]   A. Albarbar, S. Mekid, A. Starr, and R. Pietruszkiewicz, "Suitability of MEMS Accelerometers for Condition Monitoring: An experimental study," pp. 784–799, 2008.

[13]   K. S. Tee, M. Awad, A. Dehghani, D. Moser, and S. Zahedi, "Triaxial Accelerometer Static Calibration," in *World Congress on Engineering (WCE)*, 2011, vol. III, no. 2, pp. 6–9.

[14] A. Badri, J. K. Sinha, and A. Albarbar, "A Method to Calibrate the Measured Responses by MEMS Accelerometers," *Strain*, vol. 47, pp. 242–257, Dec. 2011.

[15] A. Ghosh, *Introduction to Measurements and Instrumentation*, Third Edit. New Delhi: PHI Learning Private Limited, 2009, pp. 1–810.

[16] B. Minhang, *Analysis and Design Principles of MEMS Devices*. Amsterdam, The Netherlands: ELSEVIER B. V., 2005, pp. 1–309.

[17] J. a. Plaza, a. Collado, E. Cabruja, and J. Esteve, "Piezoresistive accelerometers for MCM package," *Journal of Microelectromechanical Systems*, vol. 11, no. 6, pp. 794–801, Dec. 2002.

[18] A. Beliveau, G. T. Spencer, K. a. Thomas, and S. L. Roberson, "Evaluation of MEMS capacitive accelerometers," *IEEE Design & Test of Computers*, vol. 16, no. 4, pp. 48–56, 1999.

[19] H. Xie and G. K. Fedder, "A CMOS z-axis capacitive accelerometer with comb-finger sensing," in *Proceedings IEEE Thirteenth Annual International Conference on Micro Electro Mechanical Systems (MEMS)*, 2000, pp. 496–501.

[20] Analog-Devices, "ADXL335," 2010. [Online]. Available: www.analog.com. [Accessed: 05-Dec-2011].

[21] Carter Wind Energy, "Carter Wind Turbines." [Online]. Available: http://www.carterwindenergy.com/. [Accessed: 05-Nov-2012].

[22] Brüel & Kjær, "Instruction Manual: Impact Hammer Type 8202," 1984. [Online]. Available: http://www.titak.itu.edu.tr/Hammers_Shakers/Hammer_BK_8202.pdf. [Accessed: 05-Nov-2012].

[23] Fylde Electronics Laboratories Ltd., "FE-128 - CA Charge Amplifier Data Sheet," *Fylde Modular Instrumentation*, 2002. [Online]. Available: http://www.fylde.com/data/FE128CA.PDF. [Accessed: 05-Nov-2012].

[24] National Instruments Corporation, "M Series User Manual," 2008. [Online]. Available: http://www.ni.com/pdf/manuals/371291h.pdf. [Accessed: 10-Jul-2012].

[25] National Instruments Corporation, "NI LabVIEW SignalExpress," 2012. [Online]. Available: http://www.ni.com/labview/signalexpress/. [Accessed: 16-May-2012].

[26] MathWorks, "MATLAB: The Language of Technical Computing." [Online]. Available: http://www.mathworks.co.uk/products/matlab/. [Accessed: 01-Oct-2011].

[27] S. Thanagasundram and F. S. Schlindwein, "Comparison of integrated micro-electrical-mechanical system and piezoelectric accelerometers for machine condition monitoring," *Proceedings of the Institution of Mechanical Engineers, Part C: Journal of Mechanical Engineering Science*, vol. 220, no. 8, pp. 1135–1146, Aug. 2006.